

## Parameter identifiability of a respiratory mechanics model in an idealized preterm infant

Laura Ellwein Fix

the date of receipt and acceptance should be inserted later

**Abstract** The complexity of mathematical models describing respiratory mechanics has grown in recent years to integrate with cardiovascular models and incorporate nonlinear dynamics. However, additional model complexity has rarely been studied in the context of patient-specific observable data. This study investigates parameter identification of a previously developed nonlinear respiratory mechanics model (Ellwein Fix et al., 2018) tuned to the physiology of a 1 kg preterm infant, using local deterministic sensitivity analysis, subset selection, and gradient-based optimization. The model consists of 4 differential state equations with 34 parameters to predict airflow and dynamic pulmonary volumes and pressures generated under six simulation conditions. The relative sensitivity solutions of the model state equations with respect to each of the parameters were calculated with finite differences and a sensitivity ranking was created for each parameter and simulation. Subset selection identified a set of independent parameters that could be estimated for all six simulations. The combination of these analyses produced a subset of 6 independent sensitive parameters that could be estimated given typical clinical data. All optimizations performed using pseudo-data with perturbed nominal parameters converged within 30 iterations and estimated parameters within  $\sim 5\%$  of nominal values on average. This analysis indicates the feasibility of performing parameter estimation on real patient-specific data set described by a nonlinear respiratory mechanics model for studying dynamics in preterm infants.

---

L. Ellwein Fix  
Department of Mathematics and Applied Mathematics  
Virginia Commonwealth University  
Richmond, VA  
Tel.: +804-828-2748  
Fax: +804-828-8785  
E-mail: lellwein@vcu.edu

## 1 Introduction

Respiratory mechanics have been investigated mathematically for several decades using differential equations models that typically predict air pressure and flow in and between compartments representing aggregate features of the respiratory system. Golden et al (1973) was one of the first to develop a compartmental model of dynamic volumes and pressures in the airways, lungs, chest wall, and intrapleural space between lungs and chest wall, used to simulate a panting maneuver. Successive models built upon this foundation by including nonlinear resistances and compliances, viscoelastic components, and pulmonary circulation, and have been used to study expiratory flow limitation and energy loss (Olender et al., 1976; Liu et al., 1998; Verbraak et al., 1991; Athanasiades et al., 2000). Most recently LeRolle et al (2013) incorporated smaller diameter airways, higher respiratory rates, higher lung resistance, and higher chest wall compliances to estimate parameters using data newborn lambs. Other static computational models of breathing address the extremes of lung capacity for a single breath such as forced vital capacity maneuver or study an excised or static lung (Narusawa, 2001; Frazer et al., 2005; Uzawa et al., 2015).

We previously developed a dynamic nonlinear computational model of infant respiratory mechanics parameterized for the extremely preterm human infant (Ellwein Fix et al., 2018) to propose a mechanism of delayed progressive lung volume loss attributed to high chest wall compliance (floppiness) (Love and Tillery, 1953; Beltrand et al., 2008; Kovacs, 2015). Insufficient inhalation due to the compliant chest wall leads to decreased lung compliance and functional residual capacity, then progressive lung collapse (atelectasis), observed clinically in X-rays and by visible signs of respiratory distress that onsets after several days of stable breathing (Krauss et al., 1975; Frappell and MacFarlane, 2005; Miller et al., 2005). Ventilation assistance often fails in this population (Manley et al., 2013; Bhandari, 2013; Siew et al., 2015). Our model is the first known attempt to represent these dynamics that account for the physiology particular to premature infants, and depict the mitigating effects of expiratory laryngeal braking (grunting) and continuous positive airway pressure (CPAP) under simulated high and low chest wall compliance conditions.

With the increase in model complexity has come an increase in characterizing parameters that may number in the tens or hundreds. Simulations using nominal parameter values obtained from experimental data or population-based averages may provide insight into overall model dynamics, but model nonlinearity results in parameter values likely only valid in a local region, or the behavior of a nonlinear component being quasi-linear under a particular set of dynamic conditions. It is therefore critical to investigate which parameters most influence the model outputs under which conditions, and if any parameter dependencies or redundancies exist that may allow for simplifying model components. Parameter estimation and identification has been explored in previous respiratory models, e.g. in Le Rolle et al (2013) eight parameters characterizing compliances, resistances, and muscle activity were identified using an elementary effects algorithm on data from three newborn lambs. Parameter estimation was performed in several older linear models (Lutchen and Saidel, 1986; Avanzolini et al., 1997). There has not yet been a study that considers parameteri-

zation of a highly nonlinear pulmonary mechanics model under multiple simulation conditions.

The question of parameter identification is addressed relative to available experimental data. Typical clinical data outputs (“tracings”) for assessment of pulmonary mechanics include volumetric airflow as measured by a pneumotachograph, and pleural pressure as estimated by a pressure transducer in the esophagus. Data acquired under different experimental conditions makes it possible that a tracing from one of the two outputs may change significantly but the other output may show negligible differences, or tracings may be similar between conditions but mask different underlying dynamics. These observations may be due to operating in near-linear regions of nonlinear model constitutive equations, parameter dependencies and redundancies, and interventions impacting different components of the model. Sensitivity analysis Eslami (1994) combined with subset selection (Ipsen et al., 2011) can be used to find a set of independent sensitive parameters for which perturbations significantly impact model output. Previous studies on similar cardiovascular models include a local sensitivity analysis to reduce the size and parameter space of a compartmental model (Ellwein et al., 2008), and a comparison of healthy and elderly groups to determine differential impact of parameters (Pope et al., 2009).

The primary objective of this study is to obtain an independent sensitive parameter subset that may elucidate differences between six simulation scenarios describing the effects of grunting and CPAP during high and low chest wall compliance conditions. We begin with a brief description of the mathematical model and experimental setup. Subsequently, sensitivity analysis, subset selection, and special considerations important for analysis of breathing dynamics are described and an independent sensitive subset of candidate parameters is obtained. Finally, we test the subset in a series of gradient-based optimizations to indicate the feasibility of parameter estimation using pseudo-data generated from the simulated outputs and perturbed nominal parameter sets.

## 2 Methods

The compartmental respiratory mechanics model analyzed here (see Fig 1) was previously developed and parameterized specifically to investigate the dynamics of breathing in the extremely preterm infant weighing  $\sim 1$  kg. The naturally very high chest wall compliance of these infants has been hypothesized to be a major factor in clinically observed respiratory distress occurring in otherwise stable infants, thus the focus of the previous model was analyzing the differential impact of high vs. low chest wall compliance ( $C_w$ ) on model state outputs under the two simulated interventions of grunting (intrinsic) and CPAP (externally applied) We briefly describe the model here but also refer the reader to Ellwein et al. (2018) for full details.

### 2.1 State equations

The model describes dynamic volumes and pressures in the airways, lungs, chest wall, and intrapleural space between lungs and chest. A sigmoidal signal that repre-

Table 1: Descriptions of state variables and parameters.

Parameter/State	Physiologic description
TLC [ml]	Total lung capacity
RV [ml]	Residual volume
FRC [ml]	Functional residual capacity
VC[ml]	Vital capacity
RR [br/min]	Respiratory rate
$f$ [br/s]	Respiratory frequency
$T$ [s]	Duration of respiratory cycle
$V_T$ [ml]	Tidal volume
$\dot{V}_E$ [ml/min]	Minute ventilation
$\dot{V}_A$ [ml/s]	Airflow
$A_{mus}$ [cm H <sub>2</sub> O]	Muscle pressure amplitude
$P_{tm}$ [cm H <sub>2</sub> O]	Transmural pressure
$P_A$ [cm H <sub>2</sub> O]	Alveolar pressure
$P_{el}$ [cm H <sub>2</sub> O]	Lung elastic recoil (transpulmonary pressure)
$P_{ve}$ [cm H <sub>2</sub> O]	Viscoelastic component of pressure
$P_{l,dyn}$ [cm H <sub>2</sub> O]	Dynamic pulmonary pressure
$P_{pl}$ [cm H <sub>2</sub> O]	Pleural pressure
$P_{cw}$ [cm H <sub>2</sub> O]	Chest wall elastic recoil
$P_{mus}$ [cm H <sub>2</sub> O]	Respiratory muscle pressure
$C_A$ [ml/cm H <sub>2</sub> O]	Lung compliance
$C_w$ [ml/cm H <sub>2</sub> O]	Chest wall compliance
$C_{rs}$ [ml/cm H <sub>2</sub> O]	Respiratory system compliance
$R_{rs}$ [cm H <sub>2</sub> O s/L]	Respiratory system resistance
$v$	Fraction of VC for chest wall relaxation volume
$V_0$ [ml]	Chest wall relaxation volume
$\beta$	Baseline fraction of lung recruited at $P_{el} = 0$
$\gamma$	Maximum recruitable function of lung
$\alpha$	Lower asymptote, fraction recruitment
$k$ [1/cm H <sub>2</sub> O]	Lung elasticity coefficient
$c_F$ [cm H <sub>2</sub> O]	Pressure at maximum lung recruitment
$d_F$ [cm H <sub>2</sub> O]	Characterizes slope at maximum lung recruitment
$c_w$ [cm H <sub>2</sub> O]	Transition point, chest wall compliance
$d_w$ [cm H <sub>2</sub> O]	Chest wall compliance slope coefficient
$c_c$ [cm H <sub>2</sub> O]	Pressure at peak collapsible airway compliance
$d_c$ [cm H <sub>2</sub> O]	Collapsible airway compliance slope coefficient
$K_c$ [cm H <sub>2</sub> O s/L]	Collapsible airway resistance coefficient
$V_{c,max}$ [ml]	Peak collapsible airway volume
$R_{s,m}$ [cm H <sub>2</sub> O s/L]	Minimum small airway resistance
$R_{s,d}$ [cm H <sub>2</sub> O s/L]	Change in small airway resistance
$K_s$	Small airway resistance low pressure coefficient
$I_u$ [cm H <sub>2</sub> O s <sup>2</sup> /L]	Upper airway inertance
$R_{u,m}$ [cm H <sub>2</sub> O s/L]	Laminar value, upper airway resistance
$K_u$ [cm H <sub>2</sub> O s/L]	Turbulent coefficient, upper airway resistance
$R_{u,mult}$	Level of expiratory resistance increase
$C_{ve}$ [L / cm H <sub>2</sub> O]	Lung viscoelastic compliance
$R_{ve}$ [cm H <sub>2</sub> O s/L]	Lung viscoelastic resistance

sents a combined respiratory muscle pressure generated during spontaneous breathing drives the model. The model is designed using the volume-pressure analog of an electrical circuit, with states in terms of pressure  $P(t)$  [cm H<sub>2</sub>O] and volume  $V(t)$  [ml] in and between air compartments and with volumetric flow rate and rate of change

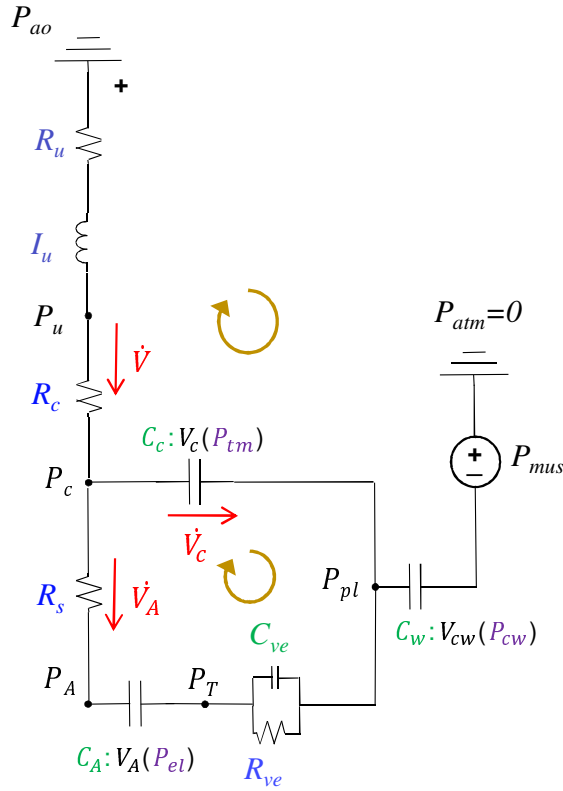


Fig. 1: Lumped-parameter respiratory mechanics model shown as its electrical analog, adapted from Ellwein Fix et al (2018). Each compliant compartment  $C$  (green) has a associated volume  $V$  is a function of the transmural pressures (purple) across the compartment boundaries. Air flows  $\dot{V}$  (red) across resistances  $R$  and inertance  $I$  (blue) are positive in the direction of the arrows. Circular yellow arrows indication direction of loop summations used to derive the system differential equations (Eq. 1). Subscripts: airway opening  $ao$ , upper  $u$ , collapsible  $c$ , small peripheral  $s$ , alveolar  $A$ , viscoelastic  $ve$ , lung elastic  $el$ , tissue  $T$ , transmural  $tm$ , pleural  $pl$ , chest wall  $cw$ , muscle  $mus$ .

of compartmental volume represented as  $\dot{V}(t)$  [ml/s] and  $\frac{dV}{dt}$  respectively. Air pressure  $P_i$  within volume  $i$  is defined relative to the external atmospheric pressure, set as  $P_{ext} = 0$ .

The pressure  $P_{ij} = P_i - P_j$  refers to the transmural pressure across a compliant boundary separating volumes  $i$  and  $j$ . Pressures  $P_{ij}$  include transmural pressure between the compliant airways and the pleural space  $P_{tm} = P_c - P_{pl}$ , lung elastic recoil  $P_{el} = P_A - P_T$ , lung viscoelastic component  $P_{ve} = P_T - P_{pl}$ , and chest wall elastic recoil  $P_{cw} = P_{pl} - P_{mus}$ . Nonlinear compliance  $C_i$  [ml/cm H<sub>2</sub>O] of a compartment is

described by  $dV_i/dt = C_i(dP_{ij}/dt)$ , resistance  $R_i$  [cm H<sub>2</sub>O·s/ml] in the airways or tissues by  $\dot{V}_i = (P_{i-1} - P_i)/R_i$ , and inertial effects  $I$  in the upper rigid airway (trachea) as  $P_{i-1} - P_i = I\dot{V}$ . Conservation laws require that  $V = V_{cw} = V_A + V_c$ , in other words the total system volume equals the chest wall volume, which is the sum of the alveolar and compressible airway volumes. The resulting system of differential equations after summing pressures over loops and incorporating compliances and resistances is given by:

$$\begin{aligned} \dot{V} : \frac{d\dot{V}}{dt} &= \frac{1}{I_u} (P_{ao} - P_u - R_u\dot{V}) & (1) \\ \dot{V}_c : \frac{dV_c}{dt} &= \dot{V} - \dot{V}_A \\ \dot{P}_{el} : \frac{dP_{el}}{dt} &= \frac{\dot{V}_A}{C_A} \\ \dot{P}_{ve} : \frac{dP_{ve}}{dt} &= \frac{\dot{V}_A - (P_{ve}/R_{ve})}{C_{ve}} \end{aligned}$$

Variable and parameter descriptions are given in Table 1. All previously developed formulations describing the nonlinear compliances and resistances are summarized in Table 2. The quantity  $C_A$  is implicitly described by  $V_A(P_{el})$  and was calculated exactly using symbolic computation as  $\partial V/\partial P$ . Breath-to-breath values for dynamic lung compliance  $C_L$  and chest wall compliance  $C_w$  are estimated during tidal breathing as  $\Delta V/\Delta P$  from the curves  $V_A(P_{el})$  and  $V_{cw}(P_{cw})$  respectively, and compared with literature to lend support to simulated outputs (see Table 3). Pressure  $P_{mus}$  describes the effective action of the respiratory muscles that drives the model dynamics, with  $P_{mus}$  negative in the outward direction.

## 2.2 Model parameters and simulation conditions

Nominal parameters for the equations in Table 2 were tuned in the original model such that resulting lung and chest wall compliance curves produced states, dynamic compliances, and FRC comparable to reported literature values. (See Ellwein Fix et al. (2018) for greater detail.) Table 4 gives parameter values in the state or constitutive equations that remain unchanged between simulations and their relevant sources and calculations. Parameters that vary specifically for each of the set of six simulation conditions are shown in Table 3. For example, the lung curve is parameterized by  $k$ ,  $\alpha$ ,  $\gamma$ ,  $c_F$ , and  $d_F$  to obtain a compliance curve with approximate slope of 2.3 ml/cm H<sub>2</sub>O (Pandit et al., 2000) during breathing with no interventions. The single degree of freedom  $d_w$  for the chest wall compliance curve differentiates between the high and low  $C_w$  conditions, where low compliance is nearly equal to lung compliance but high compliance can be approximate 5 times that (Gerhardt and Bancalari, 1980). Functional residual capacity (FRC), the volume at 0 respiratory pressure, is calculated using a nonlinear solver as the volume where static  $P_{cw} + P_{el} = 0$ , thus it takes on different values based on the chest wall compliance curve.

Simulation conditions were chosen to demonstrate the dynamics of five steady breathing cycles at respiratory rate of 60 br/min under high and low  $C_w$  conditions and

Table 2: Model functions for constitutive relations. See also Ellwein Fix et al (2018).

Description	Function
Upper airways resistance	$R_u = R_{u,m} + K_u  \dot{V} $
Collapsible airways resistance	$R_c = K_c \left( \frac{V_c, \max}{V_c} \right)^2$
Small (peripheral) airways resistance	$R_s = R_{s,d} \cdot e^{K_s(V_A - RV)/(TLC - RV)} + R_{s,m}, \quad K_s < 0$
Collapsible airways volume compliance	$V_c = \frac{V_c, \max}{1 + e^{-(P_m - c_c)/d_c}}$
Chest wall volume compliance	$V_{cw} = RV + (V_0 - RV) \ln \left( 1 + e^{P_{cw}/d_w} \right) / (\ln 2)$
Lung tissue volume compliance	$V_A = V_{el}(P_{el}) \cdot F_{rec}(P_{el}) + RV, \quad \text{where}$ $V_{el} = VC \cdot (1 - e^{(-kP_{el})}) \quad \text{and}$ $F_{rec} = \alpha + \frac{\gamma - \alpha}{1 + e^{-(P_{el} - c_F)/d_F}}$
Lung viscoelastic recoil	$C_{ve} \frac{dP_{ve}}{dt} = \dot{V}_A - P_{ve}/R_{ve}$
Diaphragm muscle driving pressure	$P_{mus} = A_{mus} \cos(2\pi ft) - A_{mus}$

Table 3: Model parameters and composite output compliances varying with chest wall compliance and simulation conditions. See Table 1 for parameter descriptions.

	High $C_w$			Low $C_w$			References
	normal $R_u$	increased $R_u$	$P_{ao} = 5$	normal $R_u$	increased $R_u$	$P_{ao} = 5$	
<i>Model Parameters</i>							
FRC	24.9	24.9	24.9	28.1	28.1	28.1	(Smith and Nelson, 1976; Donn, 1998; Thomas et al., 2004)
$A_{mus}$	1.85	3.20	2.21	2.78	3.80	2.76	—
$d_w$	0.48	0.48	0.48	2.4	2.4	2.4	—
$R_{u, mult}$	1	10	1	1	10	1	—
<i>Simulated Outputs</i>							
$C_L$	2.7	2.1	1.7	2.3	2.1	1.8	(Gerhardt and Bancalari, 1980; Mortola, 1987; Pandit et al., 2000)
$C_w$	9.9	16.0	20.4	2.7	3.3	3.9	(Gerhardt and Bancalari, 1980; Mortola, 1987)

FRC is calculated by solving  $P_{el}|_{FRC} + P_{cw}|_{FRC} = 0$ .

two simulated interventions. Grunting, simulated as increased airway resistance during expiration, is implemented by multiplying the entire  $R_u$  expression by  $R_{u, mult} = 10$  when  $\dot{V} < 0$ . CPAP is applied by an increase in  $P_{ao}$  to 5. Respiratory muscle pressure amplitude  $A_{mus}$  is set for each simulation to obtain constant tidal volume  $V_T$  of 6 ml (Pandit et al., 2000; Habib et al., 2003; Schmalisch et al., 2005) and minute ventilation  $\dot{V}_E$  of 360 ml/min (Donn, 1998).

The system of differential equations (1), together with the constitutive relations in Table 2, were solved using MATLAB R2016b (MathWorks, Natick, MA) with the differential equations solver `ode15s`. Initial conditions for  $\dot{V}$  and  $P_{ve}$  were set at 0, and for  $V_c$  was set at 0.0001 (Liu et al., 1998). Initial conditions for  $P_{el}$  were 0.954 and 2.015 for high and low  $C_w$  respectively, calculated as the pressure at which functional residual capacity was established.

Table 4: Tuned nominal steady-state and dynamic simulation parameters that remain consistent between simulations. See Table 1 for parameter descriptions.

Parameter	Value	Formula	References
TLC	63	—	Smith and Nelson (1976); Donn (1998)
RV	23	—	Smith and Nelson (1976)
VC	40	TLC-RV	Smith and Nelson (1976); Donn (1998)
RR	60	—	Donn (1998)
$f$	1	RR/60	—
$T$	1	$1/f$	—
$v$	0.25	—	Donn (1998); Goldsmith and Karotkin (2011)
$V_0$	35	$v \cdot VC + RV$	—
$\beta$	0.01	estimated	Hamlington et al. (2016)
$\gamma$	1	estimated	Hamlington et al. (2016)
$\alpha$	-0.76	$\frac{(1+e^{c_F/d_F})\beta-\gamma}{e^{c_F/d_F}}$	Hamlington et al. (2016)
$k$	0.07	estimated	Ferreira et al. (2011); Hamlington et al. (2016)
$c_F$	0.1	estimated	Hamlington et al. (2016)
$d_F$	0.4	estimated	Hamlington et al. (2016)
$c_w$	0	estimated	—
$c_c$	4.4	estimated from adult	Liu et al. (1998)
$d_c$	4.4	estimated from adult	Liu et al. (1998)
$K_c$	0.1	estimated from adult	Athanasiades et al. (2000)
$V_{c,max}$	2.5	estimated as dead space	Donn (1998); Neumann et al. (2015)
$R_{s,m}$	12	—	Ratjen and Wiesemann (1992); Singh et al. (2012)
$R_{s,d}$	20	estimated from adult	Athanasiades et al. (2000)
$K_s$	-15	estimated from adult	Athanasiades et al. (2000)
$I_u$	0.33	—	Singh et al. (2012); Le Rolle et al. (2013)
$C_{ve}$	0.005	estimated from adult	Athanasiades et al. (2000)
$R_{ve}$	20	estimated from adult	Athanasiades et al. (2000)
$R_{u,m}$	20	estimated	(Mortola, 1987; Singh et al., 2012)
$K_u$	60	estimated	(Mortola, 1987; Athanasiades et al., 2000; Singh et al., 2012)

See Table 1 (Glossary) for variable definitions and units.

### 2.3 Sensitivity analysis

Local sensitivity analysis is performed with parameter sets that characterize each of the six simulation conditions. Parameters that were kept fixed during sensitivity analysis included

$$\mu_{fix} = \{RV, TLC, FRC, VC, V_0, \alpha, v\}$$

because they were either established *a priori* for the idealized subject or known redundancies existed. The parameters

$$\mu_{vary} = \{A_{mus}, d_w, R_{u,multi}\}$$

differ between simulations while the remaining parameters are kept constant, see Tables 3 and 4. If different subsets of  $\mu = \mu_{fix} \cup \mu_{vary}$  generating different simulation conditions result in nearly similar tracings for one or both of the two outputs, the outputs may still be sensitive to different parameters in the full parameter set based on the underlying nonlinear dynamics.

We used a standard local differential equation analysis approach (Eslami, 1994) for calculating time-dependent sensitivities for each simulation and parameter, calculated a single scalar sensitivity value for each, then ranked sensitivities for each simulation condition and overall. We use non-dimensional relative sensitivities, multiplying by the parameter value and normalizing by dividing by a measure of the magnitude of the output. To avoid problems when output values are near or at 0 which would produce infinite sensitivities (such as from using the airflow time series oscillating around 0) (Bahill et al., 1980; Karnavas et al., 1993; Wu et al., 2010), we normalize using the maximum value of the output in absolute value. This gains the benefits of scaling to remove the impact of parameter units as well. Thus the relative sensitivity  $S_{ij}$  of output  $y_i$  to parameter  $\mu_j$  at nominal parameter set  $\mu_0$  is defined as

$$S_{ij}(t, \mu) \Big|_{\mu=\mu_0} = \frac{\partial y_i(t, \mu)}{\partial \mu_j} \frac{\mu_j}{\max_t y_i} \Big|_{\mu=\mu_0}. \quad (2)$$

Derivatives of  $y$  with respect to  $\mu_j$  were computed with a forward difference approximation using a difference increment of  $\epsilon_j = 1e-4$ .

To obtain a scalar value for ranking, we computed composite sensitivities  $\bar{S}_j$  using the standard 2-norm for each of the six simulations,

$$\bar{S}_j = \|S_{ij}(t, \mu)\|_2. \quad (3)$$

The sensitivities are averaged across the set of six simulations to obtain a measure of sensitivity applicable to the entire parameter space of this study. Given that this is a local analysis, we also examine rankings for each parameter between the six simulations.

#### 2.4 Subset selection

Discerning the relative impact of a parameter on output states does not identify any dependencies or redundancies between model parameters (Burth et al., 1999; Heldt, 2004; Pope et al., 2009). Identifying a set of independent parameters for the set of simulations may make future parameter estimation of patient-specific data sets more tractable and allow for reducing, linearizing, or simplifying model components. We use a validated subset selection method (Ipsen et al., 2011) that addresses the question of practical identifiability, i.e. determining a set of independent parameters that are identifiable given limited experimental output data.

The subset selection method begins by computing the singular value decomposition of the sensitivity matrix  $S|_{\mu=\mu_0} = U\Sigma V^T$  where  $\Sigma$  is a diagonal matrix of singular values in decreasing order and  $V$  contains the corresponding right singular vectors. We predict a numerical rank  $\rho$  which indicates the number of maximally independent columns of  $S$ , using a prescribed  $\epsilon$  such that  $\sigma_\rho/\sigma_1 > \epsilon \geq 10\epsilon_j$ , where  $\sigma_1$  is the largest singular value and  $\epsilon_j$  is the Jacobian finite difference approximation increment. The numerical rank is equivalent to the number of parameters that can be identified given the model output  $y_i(\mu)$  and is used to partition  $V = [V_\rho V_{n-\rho}]$  where  $n$  is the total number of parameters analyzed.

The particular parameters associated with the  $\rho$  largest singular values are found using QR-decomposition with column pivoting. The permutation matrix  $P$  that results from the decomposition  $V_\rho^T P = QR$  is applied to reorder the parameter vector  $\mu_0$  to obtain  $\tilde{\mu}_0 = P^T \mu_0$ , which is partitioned as  $\tilde{\mu}_0 = \tilde{\mu}_{0,\rho} \tilde{\mu}_{0,n-\rho}$ . The vector  $\tilde{\mu}_{0,\rho}$  then constitutes an independent set of model parameters that are estimable as part of a reduced-order minimization problem

$$\arg \min_{\mu} J(\tilde{\mu}_{0,\rho}) \quad (4)$$

where  $J$  is the least-squares cost, while parameters  $\tilde{\mu}_{0,n-\rho}$  would remain fixed at baseline estimates. in Eq. 6

## 2.5 Optimization and parameter estimation

Our objective is to obtain an independent sensitive parameter subset that may elucidate differences between the simulations described in Section 2.2 for the idealized preterm infant in Ellwein et al (2018) using tracings of airflow  $\dot{V}$  and pleural pressure  $P_{pl}$ . The two simulated tracings generated an output vector of length  $4N$ :

$$y = [\dot{V}(t_1), \dots, \dot{V}(t_{2N}), P_{pl}(t_1), \dots, P_{pl}(t_{2N})]^T \quad (5)$$

where  $N$  is the number of time points in a single breathing cycle. The third and fourth full cycles are used to ensure that transient behavior was excluded. Note that  $P_{pl}$  is not a state variable in the system of differential equations, but is obtained by  $P_{pl} = P_{cw}(V_{cw}) + P_{mus}$  where  $V_{cw} = V_A + V_c$ . Given a set of experimental or simulated patient-specific data, we aim to solve the minimization problem where  $J$  is the least-squares cost function:

$$J = \sum_{i=1}^{2N} \left| \frac{\dot{V}^d(t_i) - \dot{V}^m(t_i)}{\dot{V}_{max}^d} \right|^2 + \sum_{i=1}^{2N} \left| \frac{P_{pl}^d(t_i) - P_{pl}^m(t_i)}{P_{pl,max}^d} \right|^2$$

Superscripts  $d, m$  refer to the data and model respectively, and subscript  $max$  denotes the maximum in absolute value of each data set. The result of the minimization is a parameter set that generates model output that is the ‘‘best fit’’ to data.

To demonstrate the feasibility of estimation of an independent sensitive parameter set for this model in the absence of real data, we created psuedo-data using model output generated by simulating the forward model with the true parameter sets  $\mu^*$  for each of the six simulations. Model output was perturbed by  $\approx 2\%$  by multiplying each component by  $1 + 2 \cdot 10^{-2}r$ , where  $r$  is generated from a uniform distribution between -1 and 1. Furthermore,  $\mu^*$  for each simulation was perturbed by multiplying each parameter by a value between 0.5 and 1.5 to generate a perturbed parameter set  $\tilde{\mu}_{0,\rho}$  to be optimized. Pseudo-data and corresponding parameter sets were input into a validated bound-constrained Levenberg-Marquardt optimization algorithm (Kelley, 1999) 100 times for each of the six simulations. Mean and standard deviation of optimized parameters are reported and compared against  $\mu^*$ .

### 3 Results

Fig. 2 gives the steady-state simulated tracings for  $P_{pl}$ ,  $\dot{V}$ ,  $V_A$ ,  $P_{l,dyn}$ , and  $P_A$  for all six simulations. A typical clinical setup would only obtain data for  $P_{pl}$ ,  $\dot{V}$ , and possibly a tracing for  $V_A$  that resets to zero at each breathing cycle instead of actual end-expiratory lung volume (EELV). Note that  $\dot{V}$  tracings are nearly identical under low and high  $C_w$  conditions with and without CPAP, whereas with  $R_u$  the tracings are slightly higher and shifted right  $\sim 1$  sec. Under no intervention (black lines), decreasing  $C_w$  shifts the  $P_{pl}$  curve down by about 1 cm H<sub>2</sub>O, indicating a greater pleural pressure resulting from respiratory muscle activation and translating to higher alveolar volume. However, adding simulated CPAP to the high  $C_w$  scenario (orange lines), the maximum negative  $P_{pl}$  does not change considerably but the maximum  $P_{pl}$  at end expiration increases by about 1 cm H<sub>2</sub>O. Decreasing  $C_w$  (dotted orange line) actually puts tidal breathing in a place above  $V_0$  where  $P_{pl}$  curve shifts up.

The greatest effects from the simulated interventions can actually be seen in the tracings of  $V_A$ ,  $P_{l,dyn}$ , and  $P_A$ , though neither  $P_{l,dyn}$  nor  $P_A$  are data normally accessible clinically. The differences in  $V_A$  under interventions are all vertical shifts reflecting different EELV, which would not be captured by clinical data tracings reset to zero volume at each breath. Tracings for  $P_{l,dyn}$  qualitatively follow similar shifts as  $V_A$ . CPAP appears to greatly increase the tracing for  $P_A$  where high  $R_u$  stretches it, noting however that decreased chest wall compliance appears to have negligible effect on steady-state dynamics of  $P_A$  vs high compliance.

#### 3.1 Parameter identification

Table 5 gives the rankings for all six simulation conditions. For individual simulations, 1 is the highest ranking and 20 is the lowest. Cells are also shaded for better visualization of comparison of rankings based on simulation. Average rankings in the right-most column are reported as mean across all six simulations. Fig. 3 shows actual average sensitivities across the six simulations displayed according to declining sensitivity. It is clear from both depictions that  $\beta$ ,  $c_F$ , and  $K_c$  rank consistently as low sensitivity parameters in all simulation cases and composite. Parameter  $\gamma$  ranks overall as the most sensitive in all cases. Parameters  $k$  and  $R_{um}$  rank second and third overall respectively. The next two parameters  $A_{mus}$  and  $R_{u,mult}$  rank fourth and fifth by average ranking, but fifth and fourth by average sensitivity. A noticeable jump in average sensitivity occurs after the sixth parameter, giving the top six sensitive parameters as  $\gamma$  (maximum fractional recruitment),  $k$  (lung elasticity coefficient),  $R_{u,m}$  (laminar upper airway resistance),  $R_{u,mult}$  (level of airway braking),  $A_{mus}$  (muscle pressure amplitude), and  $d_w$  (chest wall compliance slope coefficient). A smaller jump occurs after the 8th parameter which would include  $R_{s,m}$  (minimum small airway resistance) and  $C_{ve}$  (viscoelastic compliance) as possible sensitive parameters.

Table 5 highlights several out of trend parameter-simulation combinations. Parameters  $d_F$  and  $K_s$ , which characterizes the slope of the lung recruitment function and the lung resistance, are at their most sensitive under normal breathing but drop in sensitivity under interventions. Conversely,  $c_c$  is ranked lower sensitivity without

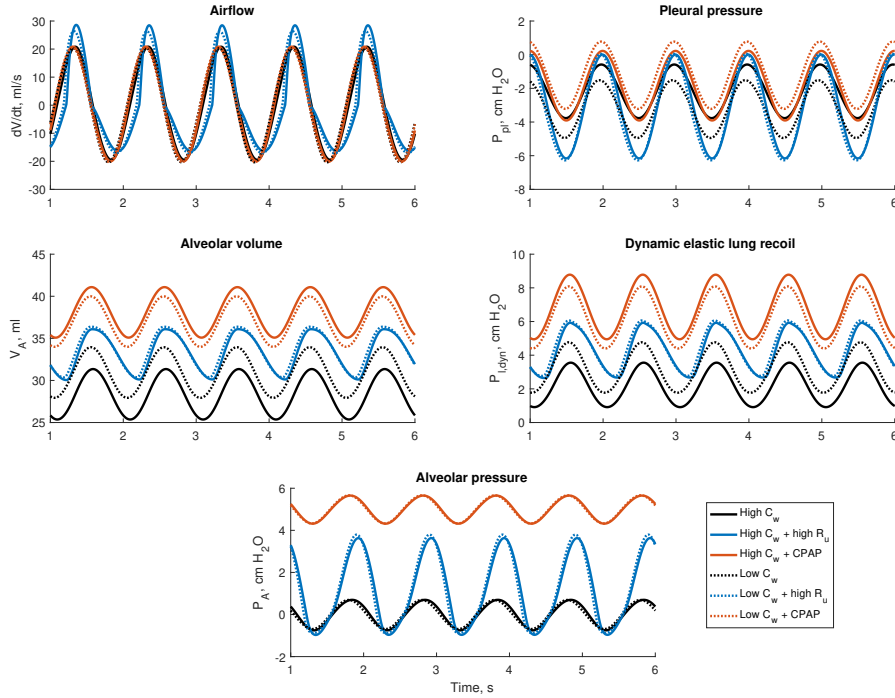


Fig. 2: Five dynamic period state variables shown in steady-state under six simulation conditions: high and low chest wall compliance, with and without CPAP and increased expired  $R_u$ .

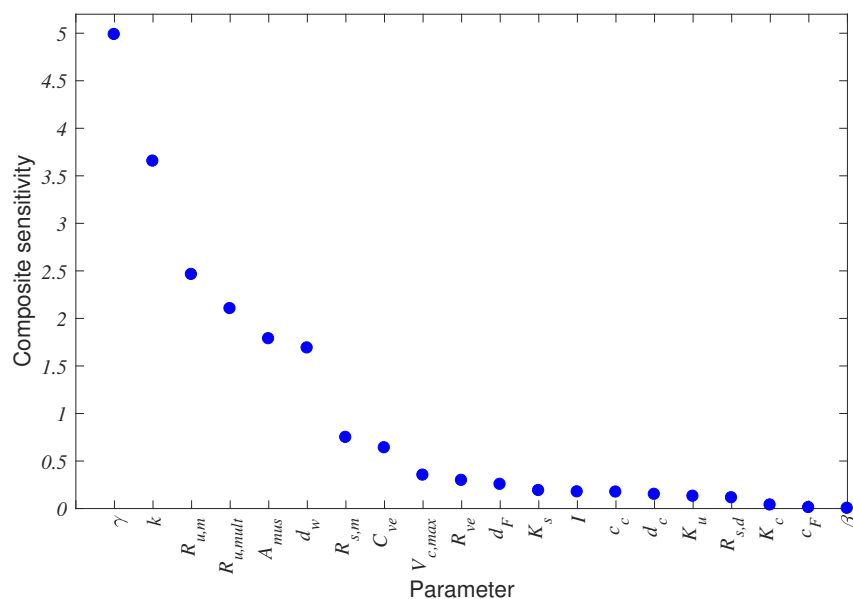
CPAP but increases ranking noticeably with CPAP, and inductance  $I$  appears to be at its most sensitive during increased  $R_u$  conditions. Finally,  $R_{s,d}$  shows medium sensitivity under normal breathing and high  $C_w$  but low sensitivity for all other simulations. These findings seem to indicate that the static respiratory compliance curves exhibit a larger influence over the breathing output during normal breathing, but influence shifts to the airway parameterization during increased  $R_u$  during expiration. These features would be masked if only the overall ranking was used to determine sensitivity, though it still remains to discuss if these low-to-mid sensitivity shifts among simulations are sensitive enough to manifest in the outputs.

Parameters that exhibit low to medium sensitivity across all simulations include  $C_{ve}$ ,  $R_{ve}$ , and  $I$ . We expect that while it would not be effective to remove lung tissue viscoelasticity and airway inertial effects from the model, the actual values of these parameters do not appear to affect the model outputs traditionally seen in experimental data and therefore could remain fixed at nominal values during an optimization.

Table 6 shows the subsets chosen for each of the six simulations, sorted in the same order as Table 5 with a line separating the top six sensitive parameters by rank-

Table 5: Sensitivity rankings for each of the six simulations with an average ranking in the right-most column. Highlighting in cells indicates relative rankings.

	High $C_w$			Low $C_w$			Average ranking
	normal $R_u$	increased $R_u$	$P_{ao} = 5$	normal $R_u$	increased $R_u$	$P_{ao} = 5$	
$\gamma$	1	1	1	1	1	1	1.0
$k$	2	4	2	3	4	2	2.8
$R_{u,m}$	4	2	3	5	2	5	3.5
$A_{mus}$	3	5	6	2	6	4	4.3
$R_{u,mult}$	6	3	4	6	3	6	4.7
$d_w$	5	6	8	4	5	3	5.2
$R_{s,m}$	7	7	5	7	7	8	6.8
$C_{ve}$	8	8	7	8	8	9	8.0
$V_{c,max}$	13	11	9	12	9	7	10.2
$R_{ve}$	12	9	10	10	10	11	10.3
$d_F$	9	12	18	9	14	17	13.2
$I$	15	10	13	17	11	14	13.3
$c_c$	16	16	11	14	13	10	13.3
$K_s$	10	15	15	11	15	15	13.5
$d_c$	14	13	14	13	16	12	13.7
$K_u$	17	14	12	16	12	13	14.0
$R_{s,d}$	11	17	16	15	17	18	15.7
$K_c$	18	18	17	18	18	16	17.5
$c_F$	19	19	20	19	19	19	19.2
$\beta$	20	20	19	20	20	20	19.8

Fig. 3: Composite sensitivities  $S_j$  averaged across the six simulations. Parameters are ordered by decreasing sensitivity

ing. We search for a subset of parameters that is independent for all or most of the six simulations, with parameter values that can distinguish between simulations. It is initially clear that  $\gamma$ ,  $k$ ,  $R_{u,mult}$ ,  $A_{mus}$ , and  $d_w$  were chosen for all simulations and should be considered a candidate for an independent subset. These describe the lung and chest wall compliance curves, the amplitude of the respiratory muscle driving pressure, and the level of airway braking.  $K_u$  is also chosen for all simulations. However, it is considered to have low sensitivity, and therefore attempts to optimize it would be both unnecessary and potentially hinder the computation. We also note that  $R_{u,m}$  is chosen for all simulations except high  $C_w$  with no interventions. Because it is also a highly sensitive parameter, we consider it as a candidate for the optimized subset. It is also interesting to see the increase in number of identifiable parameters with the addition of increased  $R_u$  on expiration, possibly because the shape of the output differs from the other two interventions.

Considered all of the above, the final independent sensitive candidate parameter set will be tested with the gradient-based Levenberg-Marquardt optimization algorithm:

$$\tilde{\mu}_{0,\rho} = \{\gamma, k, R_{u,m}, R_{u,mult}, A_{mus}, d_w\}$$

Table 6: Display of parameters chosen by subset selection for each simulation. Parameters are ordered identical to Table 5 for comparison. Note that  $K_u$  was chosen for all six simulations but is of low sensitivity.

Parameter	High $C_w$			Low $C_w$			Number chosen
	normal $R_u$	increased $R_u$	$P_{ao} = 5$	normal $R_u$	increased $R_u$	$P_{ao} = 5$	
$\gamma$	X	X	X	X	X	X	6
$k$	X	X	X	X	X	X	6
$R_{u,m}$		X	X	X	X	X	5
$R_{u,mult}$	X	X	X	X	X	X	6
$A_{mus}$	X	X	X	X	X	X	6
$d_w$	X	X	X	X	X	X	6
$R_{s,m}$		X	X		X		3
$C_{ve}$		X			X		2
$V_{c,max}$	X						1
$R_{ve}$	X	X		X	X		4
$d_F$	X	X		X	X		4
$K_s$	X	X		X	X	X	5
$I$		X			X		2
$c_c$		X	X	X	X	X	5
$d_c$		X	X		X	X	4
$K_u$	X	X	X	X	X	X	6
$R_{s,d}$	X	X	X	X	X		5
$K_c$							0
$c_F$							0
$\beta$							0

### 3.2 Optimizations

The Levenberg-Marquardt algorithm converged by either the cost function stagnating or the norm of the gradient reaching the prescribed tolerance, see Fig. 4. It also appears that the simulations with increased expired  $R_u$  had a greater fraction of optimizations that took more iterations, with several showing an increase in gradient norm before finally approaching 0, yet they all converged within 30 iterations.

Table 7 gives the mean optimized parameter values and standard deviations for each simulation, as also depicted in the histograms in Fig. 5. Histograms are organized in columns to highlight differences in the distributions. Note that  $R_{u,m}$ ,  $k$ , and  $\gamma$  are the same for all simulations but  $A_{mus}$ ,  $d_w$ , and  $R_{u,mult}$  take on different values depending on the simulation. All optimizations were able to reasonably identify values for the six parameters within  $\sim 5\%$ .

We point out some possible correlations that may still be present. Under low  $C_w$  and no intervention, mean  $R_{u,m}$  and  $k$  were at their lowest values of the six simulation conditions while  $\gamma$  and  $R_{u,mult}$  were at their highest. Since  $k$  and  $\gamma$  describe different parts of the overall lung compliance curve, and  $R_{u,m}$  and  $R_{u,mult}$  both affect model output at different portions of the breathing cycle, it is understandable that their values may be loosely correlated. Despite this, the optimizer still converged every time and values close to nominal parameters were attained.

Table 7: Mean parameter values from 100 optimization runs for each of the six simulations, reported with standard deviation (SD).

$C_w$	Intervention	Mean optimized parameter values (SD)					
		$R_{um}$	$A_{mus}$	$d_w$	$k$	$\gamma$	$R_{u,mult}$
High	none	1.850 (.002)	0.480 (.003)	0.068 (.002)	1.02 (.02)	1.01 (.01)	
	Incr exp $R_u$	20.0 (.3)	3.200 (.005)	0.479 (.011)	0.070 (.003)	1.00 (.04)	10.0 (.1)
	$P_{ao} = 5$	19.9 (.2)	2.210 (.006)	0.481 (.013)	0.070 (.003)	1.00 (.02)	1.01 (.02)
Low	none	19.2 (.4)	2.771 (.007)	2.38 (.02)	0.065 (.002)	1.06 (.03)	1.04 (.02)
	Incr exp $R_u$	19.9 (.3)	3.800 (.006)	2.40 (.01)	0.069 (.002)	1.02 (.02)	10.0 (.1)
	$P_{ao} = 5$	19.9 (.2)	2.764 (.006)	2.41 (.01)	0.070 (.001)	1.00 (.01)	1.00 (.01)

## 4 Discussion

This study showed that a combination of sensitivity analysis and subset selection can identify an independent sensitive subset of six out of 34 parameters characterizing a respiratory mechanics model under six simulation conditions. Pseudo-data generated from simulated outputs of airflow and pleural pressure were used with perturbed nominal parameters to test the ability of a gradient-based optimization algorithm to estimate parameter close to nominal values. Parameters and simulation conditions that would be quantifiable ahead of time, such as estimates of static lung volumes based on subject size or amount of ventilation assistance, were kept fixed

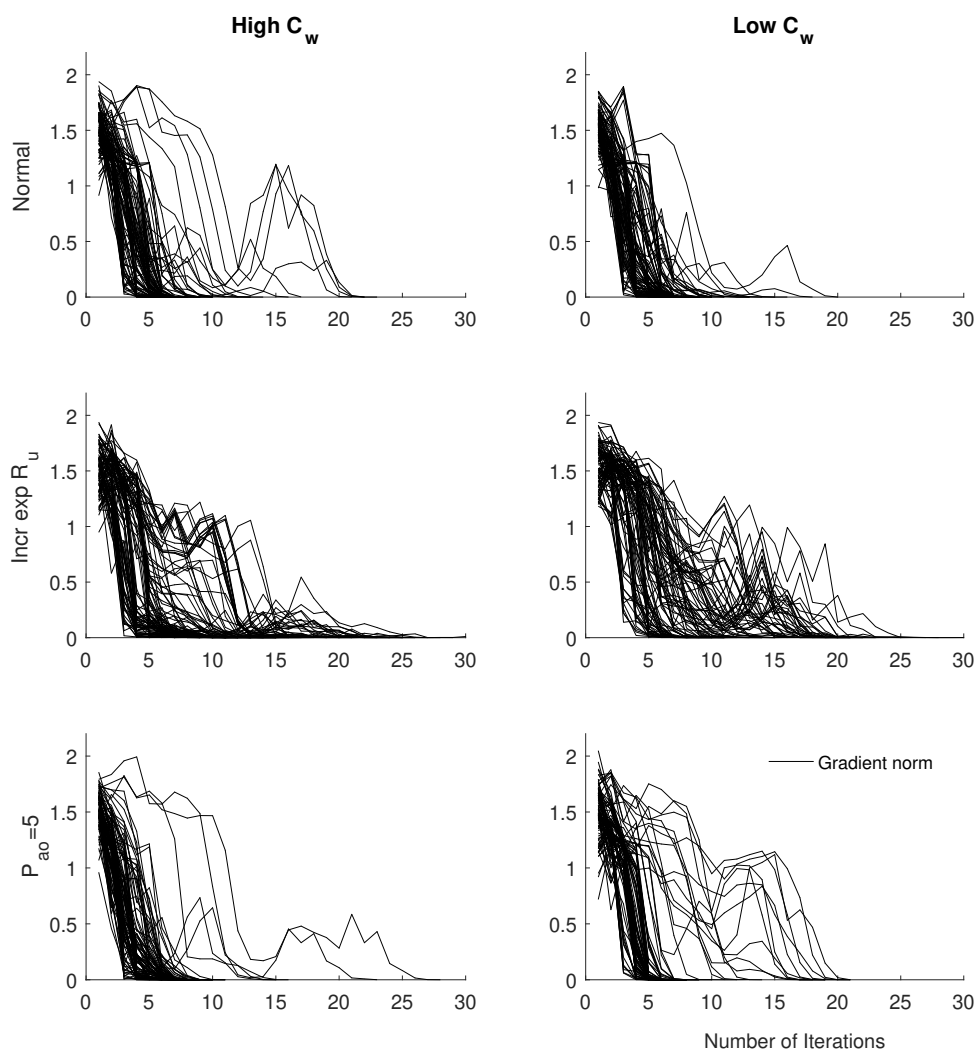


Fig. 4: Iteration histories for 100 runs for each of the six simulations. All optimizations converged within 30 iterations either by stagnated residual or gradient norm meeting the prescribed tolerance.

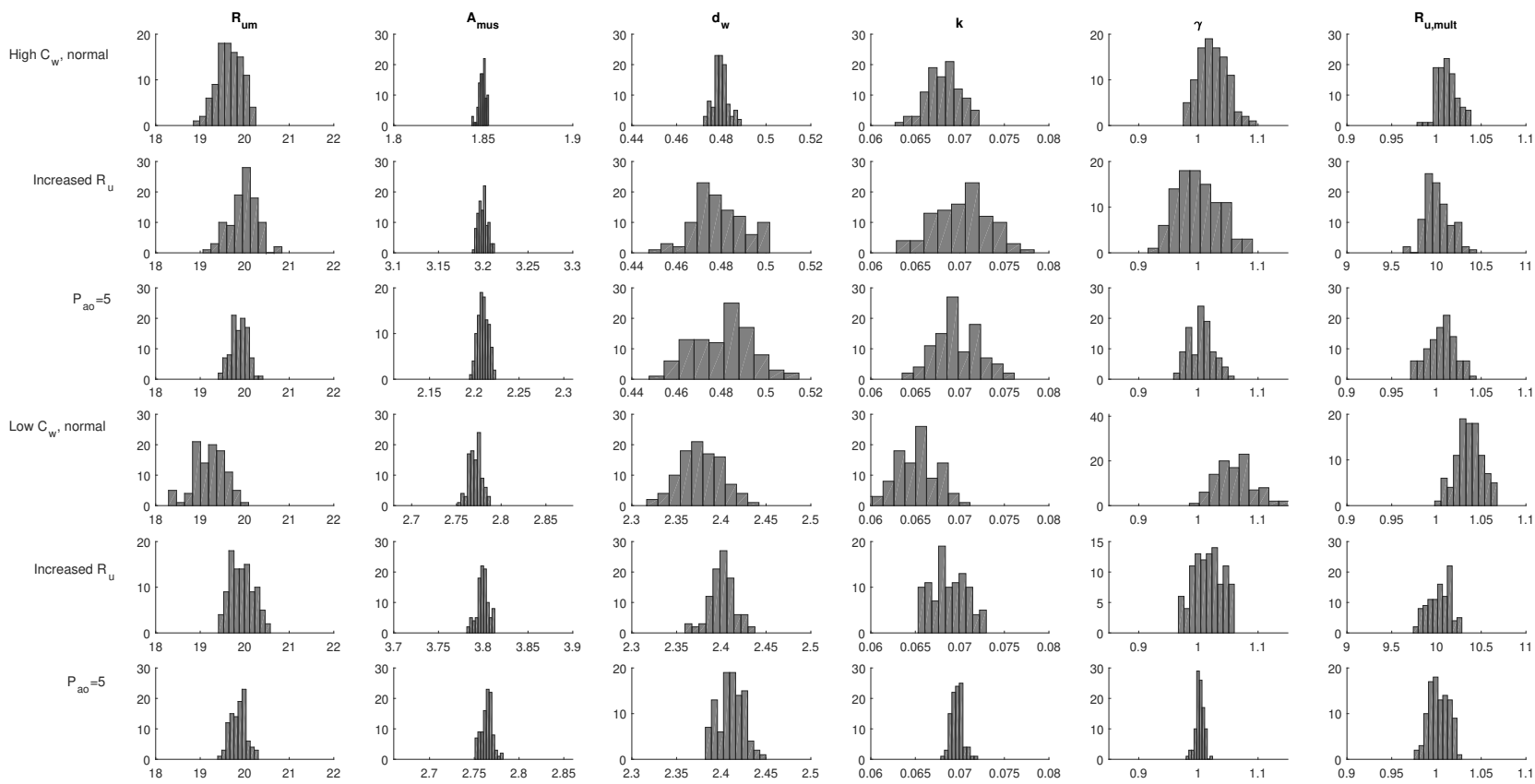


Fig. 5: Histograms for each parameter and simulation showing approximate distributions for the mean values given in Table 7.

during optimizations. Quantities like “level of grunting” quantified by  $R_{u,mult}$  or degree of chest wall compliance  $d_w$  and other parameters that differentiated between simulations were estimated computationally. This parameter set was generated in the context of light of the simulation conditions studied here; similar analyses should be conducted if experimental conditions or subject state of health changes.

Of the six most sensitive parameters as identified by composite relative sensitivities, all were chosen by subset selection as independent for all six simulations except for  $R_{u,m}$ , which was chosen for all except the high  $C_w$  normal conditions. In spite of this, the mean reported in Table 7 and the histogram in the (1,1) spot of Fig. 5 appear to fall in line with the results from the other five simulations. Because  $K_u$  was chosen as independent for all six simulations we initially included it in optimizations (results not shown). However, since the output vector  $y$  is not sensitive to  $K_u$ , its value is not critical to parameter estimation and indeed the the optimized value fluctuated greatly. All other parameters were not sensitive enough to impact the output or could not be identified in all simulations. The final parameter set  $\{\gamma, k, R_{u,m}, R_{u,mult}, A_{mus}, d_w\}$  characterizes the static respiratory compliance curves that underlie the dynamics, airway resistance, and respiratory muscle pressure amplitude.

The most insensitive parameters  $\beta$ ,  $c_F$ , and  $K_c$  were also not chosen as independent for any of the six simulations. Because  $\beta$  and  $c_F$  are part of the formula for  $\alpha$  which was kept fixed during analyses, it is consistent that those two parameters were considered both insensitive and dependent. Conversely  $d_F$  and  $\gamma$  were both chosen as somewhat and very sensitive respectively, suggesting that a nonlinear description for fractional recruitment is important in this model but not all parameters may impact model dynamics during steady-steady periodic conditions. It is likely that  $K_c$  does not have a great impact on model output because the magnitude  $R_c$  is not as critical in these simulations as  $R_u$  (upper airway resistance) and  $R_s$  (lung resistance). However, if experimental data was acquired during a condition exhibiting situation expiratory flow limitation such as obstructive pulmonary disease (Khirani et al., 2001),  $R_c$  may play a bigger role.

The applicability of these analyses is directly related to both the available data and the model construction. As stated earlier, lung volume  $V_A$  is often a piece of clinically available data, but is recorded as volume relative to FRC instead of an absolute lung volume. Any breath-to-breath changes in FRC are not captured in this data. Though the dynamic absolute  $V_A$  could not be compared against the model output as a result, tidal volume (volume inspired in a single breath) could be added to the output vector for parameter estimation against clinical data. It is important to reiterate that we only estimated parameters responsible for the steady-state periodic outputs prior to any volume loss. If data was acquired during progressive volume loss, the results would likely change. It is evident from the subset selection results from increased expired  $R_u$  that a slight change in the qualitative nature of the outputs increases the number of independent parameters.

Several features of preterm infant respiratory mechanics are not yet captured by the model and will be addressed in future modifications. These include variable frequency breathing, non-sinusoidal respiratory muscle pressure, intermittent deep breathing (sighing), variable time spend in inspiration vs. expiration, paradoxical chest movement, and chemoreflex feedback. The addition of model modifications

likely increases the parameter space, making it more critical to address the question of parameter identifiability. We will explore using these results to simplify constitutive relationships whose nonlinearity may not manifest during quiet tidal breathing typical of a newborn infant.

We focused our attention on local differential sensitivity analysis, SVD/QR-based subset selection, and gradient-based optimization, however there are numerous approaches available to study parameter identification and estimation with optimization. For example, Olufsen and Ottesen (2012) compare parameter identifiability of a model of heart rate regulation using a structured correlation method, the SVD/QR method, and model Hessian subspace method. Their work found the structured correlation method to produce the “best” subset with fewest interdependent parameters. The SVD/QR method did not give as precise parameter estimates but it much more computationally feasible. Derivative-free methods such as Nelder-Mead are available for optimization, but generally are passed by in favor of gradient-based algorithms when a differential equations system is being analyzed. Another option for future consideration is combining with latin hypercube sampling in a multi-start approach (Raue et al., 2013).

Respiratory mechanics models have been investigated for several years and many formulations exist; the current goal is the customization at the patient-specific level via parameter estimation performed on dynamic data tracings. This becomes an even greater challenge when working with a fragile population such as extremely preterm infants for whom experimental data collection is limited. This study indicates the feasibility of parameter estimation under a variety of experimental conditions. These methods will be applied to future data obtained in the NICU to estimate patient-specific parameters that may help uncover factors leading to progressive volume loss. The ability to predict volume loss could lead to prevention strategies and assist in the health and stability of the preterm infant population.

## 5 Acknowledgements

This research was supported in part by the Atlantic Pediatric Device Consortium FDA grant 5P50FD004193-07.

## References

- Athanasiades A, Ghorbel F, Jr JWC, Niranjana S, Olansen J, Zwischenberger JB, Bidani A (2000) Energy analysis of a nonlinear model of the normal human lung. *J Biol Sys* 8(2):115–139
- Avanzolini G, Barbini P, Cappello A, Cevenini G, Chiari L (1997) A new approach for tracking respiratory mechanical parameters in real-time. *Ann Biomed Eng* 25:154–163
- Bahill AT, Latimer JR, Troost B (1980) Sensitivity analysis of linear homeomorphic model for human movement. *IEEE Trans Syst Man Cybern* 10(12):924–929

- Beltrand J, Alison M, Nicolescu R, Verkauskiene R, Deghmoun S, Sibony O, Sebag G, Levy-Marchal C (2008) Bone mineral content at birth is determined both by birth weight and fetal growth pattern. *Pediatr Res* 64:86–90
- Bhandari V (2013) The potential of non-invasive ventilation to decrease bpd. *Semin Perinatol* 37(2):108–114
- Burth M, Verghese GC, VValerez-Reyes M (1999) Subset selection for improved parameter estimation in on-line identification of a synchronous generator. *IEEE Trans Power Systems* 14:218–225
- Donn SM (1998) *Neonatal and Pediatric Pulmonary Graphics*. Futura Publishing Company, Armonk, NY
- Ellwein L, Tran H, Zapata C, Novak V, Olufsen MS (2008) Sensitivity analysis and model assessment: mathematical models for arterial blood flow and blood pressure. *J Cardiovasc Eng* 8:94–108
- Ellwein Fix L, Houry J, Moores RR, Linkous L, Brandes M, Rozycki H (2018) Theoretical open loop model of respiratory mechanics in the extremely preterm infant. *PLoS ONE* 13(6):1–22, DOI 10.1371/journal.pone.0198425
- Eslami M (1994) *Theory of sensitivity in dynamic systems: an introduction*. Springer-Verlag, Berlin
- Ferreira JC, Bensenor FEM, Rocha MJJ, Salge JM, Harris RS, Malhotra A, Kairalla RA, Kacmarek RM, Carvalho C (2011) A sigmoidal fit for pressure-volume curves of idiopathic pulmonary fibrosis patients on mechanical ventilation: clinical implications. *Clinics* 66(7):1157–1163
- Frappell PB, MacFarlane PM (2005) Development of mechanics and pulmonary reflexes. *Respir Physiol Neurobiol* 149:143–154
- Frazer DG, Lindsley WG, McKinney W, Reynolds JS (2005) A model of the recruitment-derecruitment and volume of lung units in an excised lung as it is inflated-deflated between minimum and maximum lung volume. *J Biomech Eng* 135:034503
- Gerhardt T, Bancalari E (1980) Chestwall compliance in full-term and premature infants. *Acta Paediatr Scand* 69:359–364
- Golden JF, Jr JWC, Stevens PM (1973) Mathematical modeling of pulmonary airway dynamics. *IEEE Trans Biomed Eng* 20(6):397–404
- Goldsmith JP, Karotkin EH (2011) *Assisted Ventilation of the Neonate*. ClinicalKey 2012, Elsevier/Saunders
- Habib RH, Pyon KH, Courtney SE, Aghai ZH (2003) Spectral characteristics of airway opening and chest wall tidal flows in spontaneously breathing preterm infants. *J Appl Physiol* 94:1933–1940
- Hamlington KL, Smith BJ, Allen GB, Bates JHT (2016) Predicting ventilator-induced lung injury using a lung injury cost function. *J Appl Physiol* 121:106–114
- Heldt T (2004) *Computational models of cardiovascular response to orthostatic stress*. PhD thesis, Massachusetts Institute of Technology
- Ipsen I, Kelley C, Pope S (2011) Rank-deficient nonlinear least squares problems and subset selection. *SIAM J Numer Anal* 49:1244–1266
- Karnavas WJ, Sanchez PJ, Bahill AT (1993) Sensitivity analyses of continuous and discrete systems in the time and frequency domains. *IEEE Trans Syst Man Cybern* 23(2):488–501

- Kelley C (1999) *Iterative Methods for Optimization*. Society for Industrial and Applied Mathematics, Philadelphia
- Khirani S, Biot L, Eberhard A, Baconnier P (2001) Positive end expiratory pressure and expiratory flow limitation: a model study. *Acta Biotheor* 49:277–290
- Kovacs CS (2015) Calcium, phosphorus, and bone metabolism in the fetus and newborn. *Early Hum Dev* 50(11):623–628
- Krauss AN, Klain DB, Auld PA (1975) Chronic pulmonary insufficiency of prematurity (cpip). *Pediatrics* 55(1):55–58
- Le Rolle V, Samson N, Praud JP, Hernandez AI (2013) Mathematical modeling of respiratory system mechanics in the newborn lamb. *Acta Biotheor* 91(1):91–107
- Liu CH, Niranjan SC, Jr JWC, San KY, Swischenburger JB, Bidani A (1998) Airway mechanics, gas exchange, and blood flow in a nonlinear model of the normal human lung. *J Appl Physiol* 84(4):1447–69
- Love WG, Tillery B (1953) New treatment for atelectasis of the newborn. *AMA J Dis Child* 86(4):423–425
- Lutchen KR, Saidel GM (1986) Estimation of mechanical parameters in multicompartiment models applied to normal and obstructed lungs during tidal breathing. *IEEE Trans Biomed Eng* BME-33:878–887
- Manley BJ, Owen LS, Doyle LW, Andersen CC, Cartwright DW, Pritchard MA, Donath SM, Davis PG (2013) High-flow nasal cannulae in very preterm infants after extubation. *N Engl J Med* 369:1425–1433
- Miller TL, Palmer C, Shaffer TH, Wolfson MR (2005) Neonatal chest wall suspension splint: a novel and noninvasive method for support of lung volume. *Pediatr Pulmonol* 39:512–520
- Mortola JP (1987) Dynamics of breathing in newborn mammals. *Physiol Rev* 67(1):187–243
- Narusawa U (2001) General characteristics of the sigmoidal equation representing quasi-static pulmonary p-v curves. *J Appl Physiol* 91:201–210
- Neumann RP, Pillow JJ, Thamrin C, Larcombe AN, Hall GL, Schulzke SM (2015) Influence of gestational age on dead space and alveolar ventilation in preterm infants ventilated with volume guarantee. *Neonatology* 107:43–49
- Olender MF, Jr JWC, Stevens PM (1976) Analog computer simulation of maximum expiratory flow limitation. *IEEE Trans Biomed Eng* 23(6):445–452
- Olufsen M, Ottesen J (2012) A practical approach to parameter estimation applied to model predicting heart rate regulation. *J Math Biol* DOI:10.1007/s00285-012-0535-8:1–30
- Pandit PB, Pyon KH, Courtney SE, England SE, Habib RH (2000) Lung resistance and elastance in spontaneously breathing preterm infants: effects of breathing pattern and demographics. *J Appl Physiol* 88:997–1005
- Pope S, Ellwein L, Zapata C, Novak V, Kelley C, Olufsen M (2009) Estimation and identification of parameters in a lumped cerebrovascular model. *Math Biosci Eng* 6:93–115
- Ratjen FA, Wiesemann HG (1992) Variability of dynamic compliance measurements in spontaneously breathing and ventilated newborn infants. *Pediatr Pulmonol* 12:73–80

- Raue A, Schilling M, Bachmann J, Matteson A, Schelke M, Kaschek D, Hug S, Kreutz C, Harms B, Theis F, Klingmüller U, Timmer J (2013) Lessons learned from quantitative dynamical modeling in systems biology. *PLoS ONE* 8(9):1–17
- Schmalisch G, Wilitzki S, Wauer RR (2005) Differences in tidal breathing between infants with chronic lung diseases and healthy controls. *BMC Pediatrics* 5:36–45
- Siew ML, van Vonderen JJ, Hooper SB, te Pas AB (2015) Very preterm infants failing cpcp show signs of fatigue immediately after birth. *PLoS ONE* 10(6):1039–1051
- Singh R, Courtney SE, Weisner MD, Habib RH (2012) Respiratory mechanics during high-frequency oscillatory ventilation: a physical model and preterm infant study. *J Appl Physiol* 112:1105–1113
- Smith C, Nelson N (1976) *The physiology of the newborn infant*. Thomas, Springfield, IL
- Thomas MR, Rafferty GF, Limb ES, Peacock JL, Calvert SA, Marlow N, Milner AD, Greenough A (2004) Pulmonary function at follow-up of very preterm infants from the united kingdom oscillation study. *Am J Respir Crit Care Med* 69:868–872
- Uzawa Y, Otsuji M, Nakazawa K, Fan W, Yamada Y (2015) Derivation of recruitment function from the pressure-volume curve in an acute lung injury model. *Respir Physiol Neurobiol* 205:16–20
- Verbraak AFM, Bogaard JM, Beneken JEW, Hoorn E, Versprille A (1991) Serial lung model for simulation and parameter estimation in body plethysmography. *Med and Biol Eng and Comput* 29:309–317
- Wu WH, Wang FS, Chang MS (2010) Sensitivity analysis of dynamic biological systems with time-delays. *BMC Bioinformatics* 11(7):S12